



# Photocatalytic activity of nanocrystalline ZnO, $\alpha$ -Fe<sub>2</sub>O<sub>3</sub> and ZnFe<sub>2</sub>O<sub>4</sub>/ZnO

M. N. Zulfiqar Ahmed · K. B. Chandrasekhar ·  
A. A. Jahagirdar · H. Nagabhushana ·  
B. M. Nagabhushana

Received: 24 November 2014 / Accepted: 19 December 2014 / Published online: 7 January 2015  
© The Author(s) 2015. This article is published with open access at [Springerlink.com](http://Springerlink.com)

**Abstract** Nanocrystalline powders of ZnO,  $\alpha$ -Fe<sub>2</sub>O<sub>3</sub> and ZnFe<sub>2</sub>O<sub>4</sub>/ZnO were prepared by solution combustion method. The characterization of the nano powders was done by powder X-ray diffraction (PXRD), Fourier transform infrared spectroscopy (FTIR) and scanning electron microscopy (SEM). The ZnO and  $\alpha$ -Fe<sub>2</sub>O<sub>3</sub> nanopowders exhibited the wurtzite and hexagonal phases, respectively. The PXRD pattern of ZnFe<sub>2</sub>O<sub>4</sub>/ZnO indicated the spinel phase of zinc ferrite and wurtzite phase of zinc oxide. The three nanopowders were used as photocatalysts for the removal of the azodye brilliant yellow (BY) from its aqueous solution. A comparison of the results indicated that ZnFe<sub>2</sub>O<sub>4</sub>/ZnO showed better photocatalytic activity for the removal of BY than ZnO and  $\alpha$ -Fe<sub>2</sub>O<sub>3</sub>. This was attributed to the synergistic effect between ZnFe<sub>2</sub>O<sub>4</sub> and ZnO resulting in better charge separation and reducing the

electron–hole recombination. The photocatalytic activity followed the order: ZnO <  $\alpha$ -Fe<sub>2</sub>O<sub>3</sub> < ZnFe<sub>2</sub>O<sub>4</sub>/ZnO.

**Keywords** Solution combustion · ZnFe<sub>2</sub>O<sub>4</sub>/ZnO · Brilliant yellow · Photocatalytic activity · Spinel structure · SEM

## Introduction

The world is facing the problem of proper disposal of various products and by-products of dye industries. Dyes are used in industries such as textile, pulp and paper mills, leather, food and plastic industries, printing and publication, etc. Around 10,000 different commercial dyes and pigments exist. It has been reported that about 10–15 % of these dyes are released into the water after the dyeing process (Wanchanthuek and Nunrung 2011). These dyes are considered to be toxic and carcinogenic in nature. The presence of dyes in the effluents from textile, dyeing and printing industries leads to skin cancer due to photosensitization and photodynamic damage (Panwar et al. 2008). The various physical and chemical processes that are employed for the removal of dyes particularly from textile effluents include precipitation, adsorption, air stripping, flocculation, reverse osmosis and ultrafiltration. These techniques are, however, nondestructive due to the fact that they only transfer the non-biodegradable matter into sludge giving rise to new type of pollution which needs further treatment (Kansal et al. 2007).

The use of semiconductor metal oxides as photocatalysts has attracted the attention of many researchers across the world. These semiconductors possess narrow band gap energies. These semiconductors when illuminated with visible or ultraviolet light produce electron–

---

M. N. Zulfiqar Ahmed (✉)  
Department of Chemistry, HKBK College of Engineering,  
Bangalore 560045, India  
e-mail: [zulfi\\_chem@yahoo.com](mailto:zulfi_chem@yahoo.com)

K. B. Chandrasekhar  
Department of Chemistry, Jawaharlal Technological University  
Anantapur, Anantapuramu 515002, India

A. A. Jahagirdar  
Department of Chemistry, Dr. Ambedkar Institute  
of Technology, Bangalore 560056, India

H. Nagabhushana  
Department of Postgraduate Studies and Research in Physics,  
Tumkur University, Tumkur 572103, India

B. M. Nagabhushana  
Department of Chemistry, M S Ramaiah Institute of Technology,  
Bangalore 560054, India

hole pairs. The electrons move to the conduction band whereas the holes reside in the valence band. However, the fast recombination of these electron–hole pairs limits the commercial applications of this technology. It is therefore, important to prevent the electron–hole recombination to increase the photon efficiencies of the photocatalysts. The use of coupled semiconductor materials as photocatalysts is an important development to resolve the issue. A number of studies related to the photocatalytic activity of these coupled semiconductor photocatalysts have been reported. Coupled  $\text{Fe}_2\text{O}_3/\text{SnO}_2$  exhibited higher photocatalytic activity than pure  $\text{Fe}_2\text{O}_3$  and  $\text{SnO}_2$ . The increase in photocatalytic activity was attributed to the synergistic effect on the specific adsorption property and efficient electron–hole separation at the  $\text{Fe}_2\text{O}_3/\text{SnO}_2$  interface (Zhuang et al. 2008; Yu et al. 2003; Wang et al. 2002).

The photocatalytic degradation of methyl orange using  $\text{Bi}_{12}\text{TiO}_2/\text{SiO}_2/\text{NiFe}_2\text{O}_4$  in which  $\text{SiO}_2$  served as a barrier between  $\text{NiFe}_2\text{O}_4$  and  $\text{Bi}_{12}\text{TiO}_{20}$  and inhibited the injection of charges from  $\text{Bi}_{12}\text{TiO}_{20}$  to  $\text{NiFe}_2\text{O}_4$  thus increasing the photocatalytic activity has been reported in literature (Xu et al. 2007). The photocatalytic activity of  $\text{TiO}_2/\text{CeO}_2$ ,  $\text{TiO}_2/\text{WO}_3$ ,  $\text{TiO}_2/\text{SnO}_2$  and  $\text{ZnO}/\text{SnO}_2$  has also been reported (Zhongshen et al. 2009; Choi et al. 1994; Anpo and Takeuchi 2003; Zhang et al. 2010; Sakthivel and Kisch 2003). The degradation of methylene blue using nano  $\text{Cu}_2\text{O}/\text{TiO}_2$  prepared by electrokinetic system was studied (Xiu and Zhang 2009). It was reported that the presence of  $\text{Cu}_2\text{O}$  on the surface of  $\text{TiO}_2$  leads to a remarkable increase in the photocatalytic activity. The synthesis of  $\text{ZnO}/\text{MgO}$  nanocomposite by solid-state mixing and sintering at high temperature in a reducing atmosphere was also reported. The mixed oxide systems were found to possess properties that neither of the individual metal oxides possessed (Chawla et al. 2008). Coupling of two semiconductors with suitable band gap energies such as in  $\text{CdS}/\text{TiO}_2$ ,  $\text{CdS}/\text{ZnO}$ ,  $\text{TiO}_2/\text{SnO}_2$ ,  $\text{CdSe}/\text{TiO}_2$ , etc., significantly improves the selectivity and enhances the charge separation yields (Jang et al. 2008; Kim et al. 2009; Liu et al. 2007; Shvalagin et al. 2007). Core–shell  $\alpha\text{-Fe}_2\text{O}_3/\text{Fe}_3\text{O}_4$  was used for the photocatalytic degradation of methyl orange (Yang et al. 2011).  $\text{Fe}_2\text{O}_3/\text{CeO}_2$  photocatalyst has been shown to effectively remove methylene blue and Congo red dyes (Gajendra and Parida 2010).

Coupled semiconductor nanometal oxides such as  $\text{ZnO}/\text{TiO}_2$ ,  $\text{ZnO}/\text{SnO}_2$ ,  $\text{ZnO}/\text{CO}_3\text{O}_4$ ,  $\text{Zn}_2\text{TiO}_4$ ,  $\text{ZnTiO}_3$ ,  $\text{TiO}_2/\text{SnO}_2$ , etc., have been synthesized by various methods such as hydrothermal, chemical bath deposition, chemical vapor deposition, sol–gel and co-precipitation. However, many of these methods suffer from several drawbacks such as long reaction time, requirement of high reaction temperature, etc. Solution combustion synthesis is regarded as a

versatile tool for the synthesis of nanocrystalline metal oxides (Chang et al. 2003; Zhang et al. 2007; Khorrami et al. 2011; Corrias Ennas et al. 2011).

The present study was focused on the preparation of nanocrystalline  $\text{ZnO}$ ,  $\alpha\text{-Fe}_2\text{O}_3$  and coupled nanocomposite  $\text{ZnFe}_2\text{O}_4/\text{ZnO}$  by solution combustion method. The three nanopowders were used as photocatalysts for the degradation of the azodye brilliant yellow (BY) under UV light irradiation. The effect of various parameters such as pH, dosage of the photocatalyst and irradiation time was also studied. Studies showed that the coupled nanocomposite  $\text{ZnFe}_2\text{O}_4/\text{ZnO}$  exhibited better photocatalytic efficiency than the individual metal oxides  $\text{ZnO}$  and  $\alpha\text{-Fe}_2\text{O}_3$ .

## Materials and methods

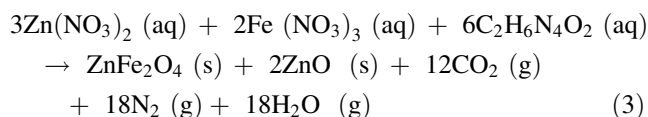
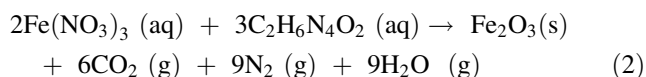
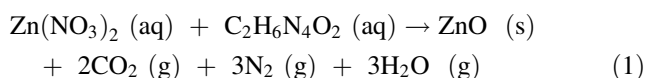
### Preparation of the nanopowders

Zinc nitrate, ferric nitrate and BY were obtained from sd Fine Chemicals Limited. The fuel oxalyldihydrazide (ODH) was prepared by the method described elsewhere (Patil et al. 2008). A 1,000 ppm stock solution of BY dye was prepared using double distilled water. The stock solution was appropriately diluted with distilled water to give solutions of concentration 10 ppm. All the reagents were of analytical grade and were used without purification. Double distilled water was used throughout the experiment.

Solution combustion synthesis involves the combustion of a fuel by an oxidizer which is usually a metal oxide. In a crystallizing dish of approximately  $300\text{ cm}^3$  capacity, appropriate amount of the metal nitrate was taken and dissolved in minimum amount of double distilled water followed by the addition of appropriate amount of the fuel. The mixture was stirred magnetically for about 10 min and the crystallizing dish was then placed on a hot plate to evaporate the excess water until a pasty mass was left. The crystallizing dish was then introduced into a muffle furnace maintained at about  $350^\circ\text{C}$ . It was observed that the mixture first dehydrated and then ignited at one spot thus initiating the combustion. The combustion process was found to be completed within a few min resulting in the formation of the nanopowder. The powder was then cooled to room temperature and ground well.

In the case of  $\text{ZnO}$  nanopowder, the oxidizer was zinc nitrate,  $\text{Zn}(\text{NO}_3)_2 \cdot 6\text{H}_2\text{O}$  whereas in the case of  $\alpha\text{-Fe}_2\text{O}_3$  nanopowder, ferric nitrate,  $\text{Fe}(\text{NO}_3)_3 \cdot 9\text{H}_2\text{O}$  was used as the oxidizer. In the case of  $\text{ZnFe}_2\text{O}_4/\text{ZnO}$  nanopowder, a mixture zinc nitrate and ferric nitrate ( $\text{Zn}/\text{Fe} \sim 1.6$ ) was used as the oxidizer.

The chemical reactions of the redox mixtures yielding the three nanopowders can be represented by Eqs. (1–3).



#### Characterization of the nanopowders

The phase purity and crystal structure of the three nanopowders were determined by powder X-ray diffraction (PXRD). The PXRD data was recorded using a Philips X'Pert pro X-ray diffractometer using Cu K $\alpha$  radiation ( $\lambda = 1.5418 \text{ \AA}$ ) at 40 kV. The mean crystallite size of the nanopowders was calculated using Eq. 4 known as the Scherer's formula (Madhusudhana et al. 2012).

$$D = \frac{k\lambda}{\beta \cos\theta} \quad (4)$$

where  $D$  is the mean crystallite size,  $k$  is a constant,  $\lambda$  is the wavelength of the X-rays used,  $\beta$  is the full width at half maximum and  $\theta$  is the Bragg's angle.

The various chemical groups present in the nanopowders were identified by Fourier transform infrared spectroscopy (FTIR). The FTIR spectra were recorded using Perkin-Elmer spectrometer (spectrum 1000) with KBr as reference.

The surface morphology of the nanopowders was determined by scanning electron microscopy (SEM). The SEM micrographs of the nanopowders were recorded using JEOL-2100F (Japan) scanning electron microscope.

#### Photocatalytic experiments

The molecular formula of BY is  $\text{C}_{26}\text{H}_{18}\text{N}_4\text{Na}_2\text{O}_8\text{S}_2$ . Chemically it is 2,2'-(1,2-ethenediyl)bis[5-[(4-hydroxyphenyl)azo]-benzene sulfonic acid disodium salt with molecular mass equal to 624.56. BY is an azo dye and its structure is shown in Fig. 1. The absorption spectrum of the dye is shown in Fig. 2. The maximum absorbance was

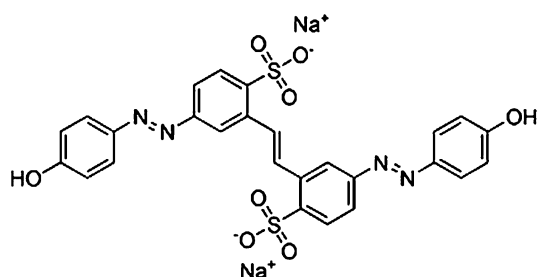


**Fig. 1** Structure of brilliant yellow

observed at 405 nm. The potential health effects of BY include irritation of the eyes and skin. Ingestion of the dye causes gastrointestinal irritation with nausea, vomiting and diarrhea. Inhalation causes irritation of the respiratory tract. Prolonged or repeated skin contact causes dermatitis.

Prior to photocatalytic experiments, studies were carried out separately to know the extent of adsorption of the dye by each of the three nanopowders in the dark. 50 cm<sup>3</sup> of the 10 ppm dye solution was transferred to the reaction vessel. 50 mg of the photocatalyst was added to it and the suspension was stirred magnetically in the dark for about 30 min. The solution was then centrifuged at 3,000 rpm for about 10 min using Remi C8C centrifuge and the UV-visible spectrum was recorded from 190 nm to 600 nm using ELICO SL-159 UV-visible spectrophotometer. It was found that in case of all the three nanopowders, there was negligible degradation of the dye under dark conditions.

The photocatalytic experiments were carried out in a reaction vessel of 500 cm<sup>3</sup> capacity with a circumference of 25.2 cm and an exposure area of 50.3 cm<sup>2</sup>. The source of UV light was a 25 W mercury vapor lamp. The distance between the surface of the solution and the mercury lamp was around 20 cm. 50 cm<sup>3</sup> of the dye solution was transferred into the reaction vessel and appropriate amount of the photocatalyst was added to it. The suspension was stirred magnetically in the dark for about 15 min to achieve adsorption-desorption equilibrium though there was negligible dye degradation in the dark. It was then exposed to UV light with constant stirring for about 30 min. It was then filtered and centrifuged at 3,000 rpm for about 10 min and the UV-visible spectrum was recorded as described earlier.

#### Effect of variable factors

The effect of pH on the photocatalytic degradation of the dye was studied by measuring the absorbance of the dye at various pH values ranging from pH 2 to 12.

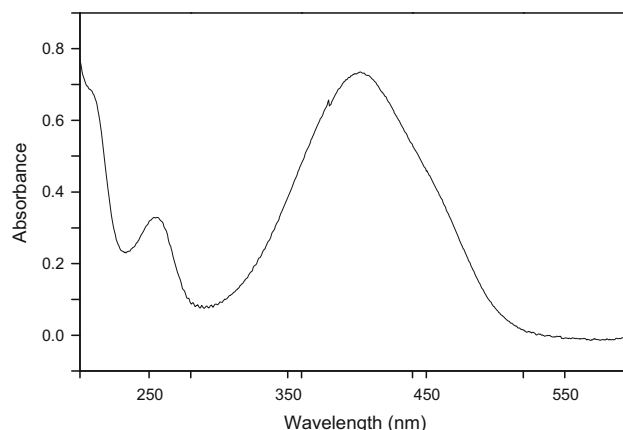


**Fig. 2** Absorption spectrum of brilliant yellow

The effect of dosage of the nanopowder was studied by varying the amount of each of the nanopowder from 0.2 to 1.6 g L<sup>-1</sup>. From the results it was observed that ZnFe<sub>2</sub>O<sub>4</sub>/ZnO nanopowder exhibited highest photocatalytic activity. The effect of irradiation time was, therefore, studied only for ZnFe<sub>2</sub>O<sub>4</sub>/ZnO.

To study the effect of irradiation time on the rate of photocatalytic degradation, 50 cm<sup>3</sup> of the dye solution was taken in the reaction vessel. Optimum amount of the ZnFe<sub>2</sub>O<sub>4</sub>/ZnO nanopowder was added to it and the suspension was stirred magnetically in the dark for about 15 min to achieve the adsorption–desorption equilibrium. The reaction vessel was then exposed to UV light with constant stirring of the suspension. After every 5 min, a small aliquot of the suspension was taken out, centrifuged, filtered and the UV–visible spectra were recorded for each aliquot. The experiment was performed for an irradiation time of up to 120 min.

## Results and discussion

The PXRD patterns of the three nanopowders are shown in Fig. 3. The peaks in the Fig. 3a correspond to the wurtzite phase of ZnO ( $a = 3.249$  Å,  $c = 5.206$  Å, JCPDS file number: 36-1451). The peaks in the Fig. 3b correspond to the hexagonal phase of  $\alpha$ -Fe<sub>2</sub>O<sub>3</sub> ( $a = 5.00$  Å,  $c = 13.62$  Å, JCPDS file number: 84-0311). In Fig. 3c the peaks at (111), (220), (311), (222), (400), (422), (511), (440) and (620) correspond to the spinel phase of ZnFe<sub>2</sub>O<sub>4</sub> ( $a = 8.4411$  Å, JCPDS file number: 22-1012) whereas the peaks at (100), (002) and (102) correspond to the wurtzite phase of ZnO ( $a = 3.249$  Å,  $c = 5.206$  Å,

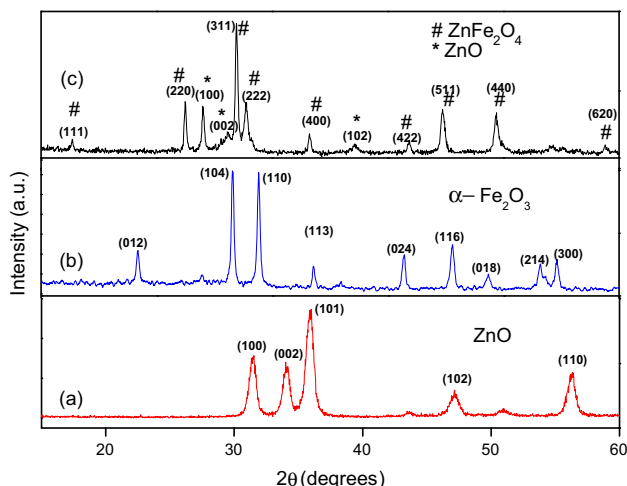


**Fig. 3** PXRD pattern of, **a** ZnO nanopowder, **b**  $\alpha$ -Fe<sub>2</sub>O<sub>3</sub> nanopowder and **c** ZnFe<sub>2</sub>O<sub>4</sub>/ZnO nanocomposite

JCPDS file number: 36-1451). It was, therefore, concluded that the compound is the coupled metal oxide ZnFe<sub>2</sub>O<sub>4</sub>/ZnO with both zinc ferrite and zinc oxide phases (Azadeh et al. 2011; Hua and Gengsheng 2009; Ping et al. 2011). It can be considered to be a core shell-coupled nanocomposite with ZnFe<sub>2</sub>O<sub>4</sub> forming the core and ZnO the shell (Chaudhuri and Paria 2012). All the three nanopowders exhibited high degree of crystallinity. No impurity peaks were detected in the PXRD patterns of all the three nanopowders.

The FTIR spectra of the three nanopowders are shown in Fig. 4. The FTIR spectrum of the ZnO nanopowder shown in Fig. 4a shows only one significant peak at around 429 cm<sup>-1</sup> that can be ascribed to the characteristic vibrational mode of Zn–O bond. The peaks at around 446 and 540 cm<sup>-1</sup> in Fig. 4b can be ascribed to the characteristic vibrations of the Fe–O bond. The FTIR spectrum of ZnFe<sub>2</sub>O<sub>4</sub>/ZnO nanopowder is shown in Fig. 4c. The peak due to Zn–O bond was shifted to around 352 cm<sup>-1</sup> whereas the peaks due to Fe–O bond were shifted to around 416 and 542 cm<sup>-1</sup>. The shift in the peaks of Zn–O peak and the Fe–O may be attributed to the change in particle size and hence the metal ion–oxygen bond distances (Thomas and George 2009; Ladgaonkar et al. 2002). The peaks at around 3400–3500 cm<sup>-1</sup> in the FTIR spectra can be ascribed to the –OH group of water adsorbed on the surface of the nanopowders (Sumetha 2008; Darezereshki 2011).

The SEM micrograph of the ZnO nanopowder is shown in Fig. 5a. The particles are nearly spherical, agglomerated and dumbbell in shape. It is also observed that the powdered products are voluminous, porous and weakly agglomerated. The SEM micrograph of the  $\alpha$ -Fe<sub>2</sub>O<sub>3</sub> nanopowder is shown in Fig. 5b. The particles are agglomerated and have irregular shape with a large number of voids. The SEM micrograph of ZnFe<sub>2</sub>O<sub>4</sub>/ZnO nanopowder shown in Fig. 5c shows that the particles have flake-like morphology and high degree of porosity.

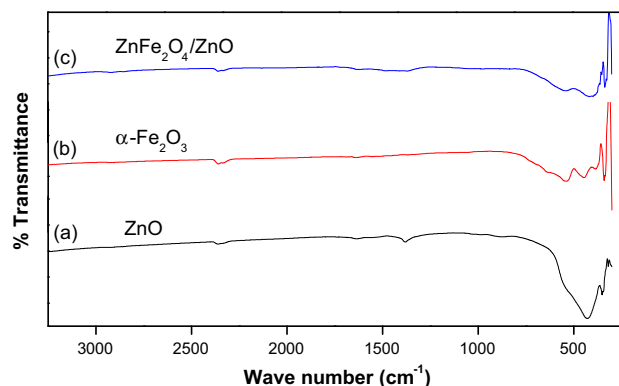


**Fig. 4** FTIR spectrum of, **a** ZnO, **b**  $\alpha$ -Fe<sub>2</sub>O<sub>3</sub> and **c** ZnFe<sub>2</sub>O<sub>4</sub>/ZnO

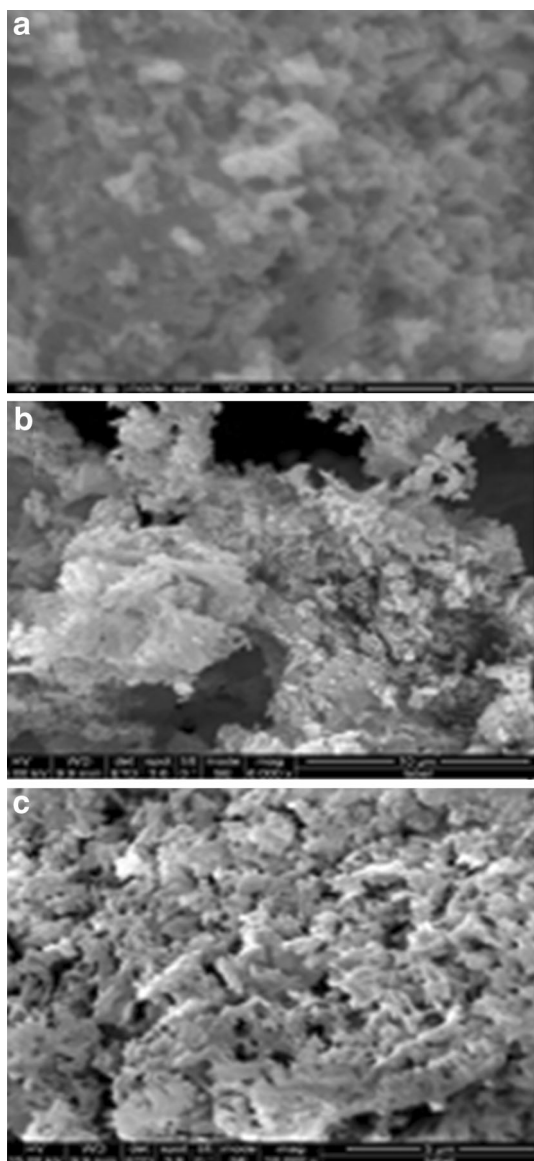


**Fig. 5** SEM micrograph of, **a** ZnO, **b**  $\alpha$ -Fe<sub>2</sub>O<sub>3</sub> and **c** ZnFe<sub>2</sub>O<sub>4</sub>/ZnO

In solution combustion synthesis, the morphological characteristics of the prepared powders are strongly dependent on the heat and gases generated during the complex decomposition. Large volumes of gases facilitate the formation of tiny particles while the heat released is an important factor for crystal growth. The porosity is high in the case of ZnFe<sub>2</sub>O<sub>4</sub>/ZnO compared to ZnO and  $\alpha$ -Fe<sub>2</sub>O<sub>3</sub> nanopowder. This can be attributed to the liberation of comparatively large volumes of gases during the formation of ZnFe<sub>2</sub>O<sub>4</sub>/ZnO nanopowder than in the case of the latter two. The agglomeration of the nanoparticles is usually considered as a common way to minimize their surface free energy (Jahagirdar et al. 2011; Zou et al. 1997).

The effect of pH on the photocatalytic degradation of BY is shown in Fig. 6. The maximum degradation

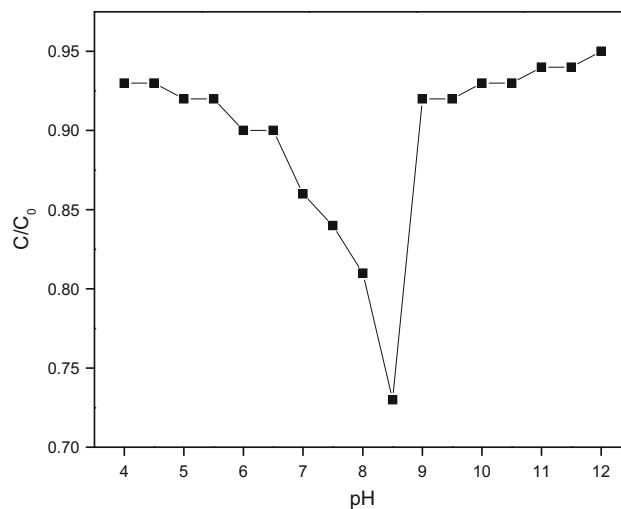


**Fig. 6** Effect of pH

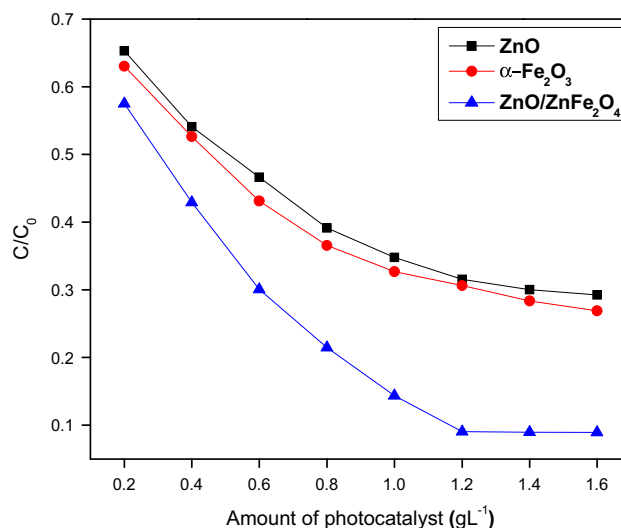


**Fig. 7** Effect of dosage of photocatalyst

was observed at pH 8.5. Hence the optimum pH was selected as 8.5.

The effect of dosage of the nanopowders on the rate of photocatalytic degradation is shown in Fig. 7. From Fig. 7, it can be concluded that the rate of photocatalytic degradation increases with increase in the amount of the nanopowder. This is due to the fact that, an increase in the amount of nanopowder increases the number of active sites thus adsorbing more number of dye molecules on the surface. It was found that ZnFe<sub>2</sub>O<sub>4</sub>/ZnO nanocomposite exhibited maximum efficiency in the removal of BY followed by  $\alpha$ -Fe<sub>2</sub>O<sub>3</sub> and ZnO. In the case of ZnFe<sub>2</sub>O<sub>4</sub>/ZnO, the optimum dosage was 1.2 g of the nanopowder per liter of the dye solution. The percentage of BY degraded by ZnO,  $\alpha$ -Fe<sub>2</sub>O<sub>3</sub> and ZnFe<sub>2</sub>O<sub>4</sub>/ZnO is 68.43, 69.36 and 90.95,



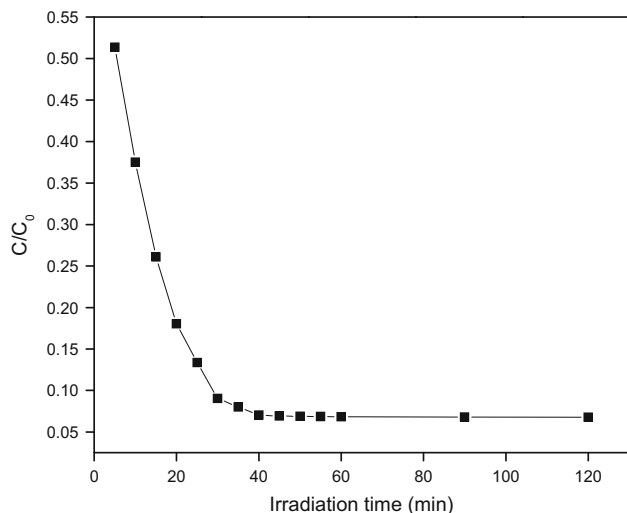


**Fig. 8** Effect of irradiation time

respectively. A further increase in the amount of the nanopowder beyond  $1.2 \text{ g L}^{-1}$  in case of  $\text{ZnFe}_2\text{O}_4/\text{ZnO}$  resulted in negligible increase in photocatalytic degradation. This can be ascribed to the fact that at higher concentration of the nanopowder, scattering of the UV radiation occurs as well as the penetration of the radiation into the dye solution also gets reduced.

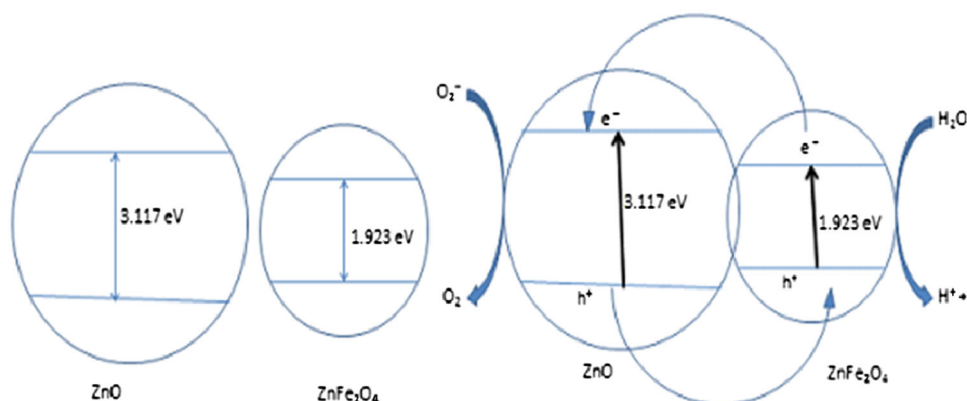
The degradation efficiency (%) of BY was calculated using Eq. 5 (Ibhadon et al. 2008).

$$\text{Degradation efficiency (\%)} = \frac{(C_0 - C_e) \times 100}{C_0} \quad (5)$$

where  $C_0$  and  $C_e$  are the initial and equilibrium concentrations of the dye.

The effect of irradiation time on the rate of photocatalytic degradation by  $\text{ZnFe}_2\text{O}_4/\text{ZnO}$  nanocomposite is shown in Fig. 8. It was found that the maximum degradation of the dye occurred at 40 min of irradiation. Beyond this, the degradation was negligible.

**Fig. 9** Mechanism of photocatalysis by  $\text{ZnFe}_2\text{O}_4/\text{ZnO}$



### Mechanism of the degradation of brilliant yellow by $\text{ZnFe}_2\text{O}_4/\text{ZnO}$

On irradiation with UV light, both the semiconductors  $\text{ZnO}$  and  $\text{ZnFe}_2\text{O}_4$  in  $\text{ZnFe}_2\text{O}_4/\text{ZnO}$  nanocomposite are excited. The band gap energy of  $\text{ZnO}$  is more than that of  $\text{ZnFe}_2\text{O}_4$ . The electrons present in the valence band of  $\text{ZnFe}_2\text{O}_4$  are promoted to its conduction band from where they are injected into the conduction band of  $\text{ZnO}$ . This results in a high concentration of electrons in the conduction band of  $\text{ZnO}$ . The holes generated in the valence band of  $\text{ZnO}$  move to the valence band of  $\text{ZnFe}_2\text{O}_4$  thus creating a high concentration of holes in it. This makes the charge separation more efficient and hence electrons and holes migrate to the surfaces of the respective particles and participate in the redox reactions around the surfaces as shown in Fig. 9. This results in an improvement in the photocatalytic activity. Hence, it can be concluded that the presence of  $\text{ZnO}$  in  $\text{ZnFe}_2\text{O}_4/\text{ZnO}$  nanocomposite improves the photocatalytic activity mainly by increasing the electron hole separation. This type of interparticle charge transfer has also been reported in case of  $\text{Nb}_2\text{O}_5/\text{SrNb}_2\text{O}_6$  nanocomposite (Xing et al. 2008).

### Conclusions

$\text{ZnO}$ ,  $\alpha\text{-Fe}_2\text{O}_3$  and  $\text{ZnFe}_2\text{O}_4/\text{ZnO}$  were successfully prepared by solution combustion method. The three nanometal oxides were used as photocatalysts for the removal of BY dye from its aqueous solution. A comparison of the results showed that the coupled nanocomposite  $\text{ZnFe}_2\text{O}_4/\text{ZnO}$  exhibited better photocatalytic efficiency for the removal of BY from aqueous solutions compared to  $\text{ZnO}$  and  $\alpha\text{-Fe}_2\text{O}_3$ . The photocatalytic process was found to be dependent on pH of the dye solution, dosage of the photocatalyst and the irradiation time.  $\text{ZnFe}_2\text{O}_4/\text{ZnO}$  can be used for effective

removal of dyes from textile and paper effluents. The increased photocatalytic activity of ZnFe<sub>2</sub>O<sub>4</sub>/ZnO nanocomposite was attributed to the increase in electron–hole separation due to interparticle charge transfer between ZnO and ZnFe<sub>2</sub>O<sub>4</sub>.

**Acknowledgments** The authors gratefully acknowledge the support rendered by the TEQIP Laboratory of M. S. Ramaiah Institute of Technology, Bangalore by providing the facilities to carry out the research work. MNZA is thankful to Dr. Sanaulla P.F, Head, Department of Chemistry; Dr. Syed Abu Sayeed Mohammed, Head, Department of Civil Engineering; the Principal and Management of HKBK College of Engineering, Bangalore for encouragement and support.

**Open Access** This article is distributed under the terms of the Creative Commons Attribution License which permits any use, distribution, and reproduction in any medium, provided the original author(s) and the source are credited.

## References

- Anpo M, Takeuchi M (2003) The design and development of highly reactive titanium oxide photocatalysts operating under visible light irradiation. *J Catal* 216:505–516
- Azadeh A, Mohammad Amin A, Ali Morsali (2011) Sonochemically assisted synthesis of ZnO nanoparticles: a novel direct method. *Iran J Chem Chem Eng* 30:75–81
- Chang YS, Chang YT, Chen IG, Chen GJ, Chai YI, Wu S, Fang TH (2003) The structure and properties of zinc titanate doped with strontium. *J Alloys Comp* 354:303–309
- Chaudhuri RG, Paria S (2012) Core–shell nanoparticles: classes, properties, synthesis mechanisms, characterization and applications. *Chem Rev* 112:2373–2433
- Chawla S, Jayanthi K, Chander H, Haranath D, Halder SK, Kar M (2008) Synthesis and optical properties of ZnO/MgO nanocomposites. *J Alloys Comp* 459:457–460
- Choi W, Termin A, Hoffman MR (1994) The role of metal ion dopants in quantum-sized TiO<sub>2</sub>: correlation between photoreactivity and charge carrier recombination dynamics. *J Phy Chem* 98:13669–13679
- Corrias Ennas G, Musinu A, Paschina G, Zedda D (2011) Iron-silica and nickel-silica nanocomposites prepared by high energy ball milling. *J Mater Res* 12:2767–2772
- Darezreshki E (2011) One-step synthesis of hematite ( $\alpha$ -Fe<sub>2</sub>O<sub>3</sub>) nano-particles by direct thermal-decomposition of maghemite. *Mater Lett* 65:642–645
- Gajendra KP, Parida KM (2010) Fabrication of iron-cerium mixed oxide: an efficient photocatalyst for dye degradation. *Int J Eng Sci Tech* 2:53–65
- Hua J, Gengsheng J (2009) Hydrothermal synthesis and characterization of monodisperse  $\alpha$ -Fe<sub>2</sub>O<sub>3</sub> nanoparticles. *Mater Lett* 63:2725–2777
- Ibhadon AO, Greenway GM, Yue Y, Falaras P, Tsoukleris D (2008) The photocatalytic activity and kinetics of the degradation of an anionic azo-dye in a UV irradiated porous titania foam. *Appl Catal B: Environ* 84:351–355
- Jahagirdar AA, Zulfiqar Ahmed MN, Donappa N, Nagabhushana H, Nagabhushana BM (2011) Synthesis, characterization and dye degradation activity of  $\alpha$ -Fe<sub>2</sub>O<sub>3</sub>. *IJETA-ETS* 5:144–147
- Jang JS, Choi SH, Kim HG, Lee JS (2008) Location and state of Pt in platinumized CdS/TiO<sub>2</sub> photocatalysts for hydrogen production from water under visible light. *J Phy Chem C* 112:17200–17205
- Kansal SK, Singh M, Sud D (2007) Studies on photodegradation of two commercial dyes in aqueous phase using different photocatalysts. *J Hazard Mater* 141:581–590
- Khorrami S, Gharib F, Mahmoudzadeh G, Sadat Sepehr S, Sadat Madani S, Naderfar N, Manie S (2011) Synthesis and characterization of nanocrystalline spinel zinc ferrite prepared by sol-gel auto combustion technique. *Int J Nano Dim* 1:221–224
- Kim JY, Choi SB, Noh JH, Yoon SH, Lee S, Noh TH, Frank AJ, Hong KS (2009) Synthesis of CdSe–TiO<sub>2</sub> nanocomposites and their applications to TiO<sub>2</sub> sensitized solar cells. *Langmuir* 25:5348–5351
- Ladgaonkar BP, Kolekar CB, Vaingankar AS (2002) Infrared absorption spectroscopic study of Nd<sup>3+</sup> substituted Zn–Mg ferrites. *Bull Mater Sci* 25:351–354
- Liu Z, Sun DD, Peng G, Leckie JO (2007) An efficient bicomponent TiO<sub>2</sub>/SnO<sub>2</sub> nanofiber photocatalyst fabricated by electrospinning with a side-by-side dual spinneret method. *Nano Lett* 7:1081–1085
- Madhusudhana N, Kambalagere Y, Kittappa MM (2012) Photocatalytic degradation of violet GL2B azo dye by using calcium aluminate nanoparticle in presence of solar light. *Res J Chem Sci* 2:72–77
- Panwar OP, Kumar A, Ameta R, Ameta SC (2008) Use of zirconium phosphate system as a photocatalyst: photobleaching of tolonium chloride. *Maced J Chem Chem Eng* 27:133–139
- Patil KC, Hegde MS, Tanu R, Aruna ST (2008) Chemistry of nanocrystalline oxide materials: combustion synthesis, properties and applications. World Scientific, Singapore, p 332
- Ping H, Dean P, Xin-feng W, Jian-jun T, Jian W, Shen-gen Z, Alex AV (2011) *J Magn Magn Mater* 323:569–573
- Sakthivel S, Kisch H (2003) Daylight photocatalysis by carbon-modified titanium dioxide. *Angew Chem Int Ed* 42:4908–4911
- Shvalagin VV, Stroyuk AL, Kotenko IE, Kuchmii SY (2007) Photocatalytic formation of porous CdS/ZnO nanospheres and CdS nanotubes. *Theor Exp Chem* 43:229–234
- Sumetha S (2008) Structural and optical properties of nanocrystalline ZnO powder from sol-gel method. *Sci Asia* 34:31–34
- Thomas Marykutty, George KC (2009) Infrared and magnetic study of nanophase zinc ferrite. *Indian J Pure Appl Phys* 47:81–86
- Wanchanthuek R, Nunrung W (2011) The adsorption study of methylene blue onto MgO from various preparation methods. *J Environ Sci Technol* 4:534–542
- Wang C, Zhao JC, Wang XM, Mai BX, Sheng GY, Peng PA, Fu JM (2002) Preparation, characterization and photocatalytic activity of nano-sized ZnO/SnO<sub>2</sub> coupled photocatalysts. *Appl Catal B: Environ* 39:269–279
- Xing J, Shan Z, Li K, Bian J, Lin X, Wang W, Huang F (2008) Photocatalytic activity of Nb<sub>2</sub>O<sub>5</sub>/SrNb<sub>2</sub>O<sub>6</sub> heterojunction on the degradation of methyl orange. *J Phys Chem Solids* 69:23–28
- Xiu FR, Zhang FS (2009) Preparation of nano-Cu<sub>2</sub>O/TiO<sub>2</sub> photocatalyst from waste printed circuit boards by electrokinetic process. *J Hazard Mater* 172:1458–1463
- Xu S, Shangguan W, Yuan J, Shi J, Chen M (2007) Preparations and photocatalytic degradation of methyl orange in water on magnetically separable Bi<sub>12</sub>Ti<sub>20</sub> supported on nickel ferrite. *Sci Technol Adv Mater* 8:40–46
- Yang T, Di W, Xiao J, Binbin Y, Sihui Z (2011) Core shell nanostructures of  $\alpha$ -Fe<sub>2</sub>O<sub>3</sub>/Fe<sub>3</sub>O<sub>4</sub>: synthesis and photocatalysis for methyl orange. *J Nanomater* 2011:1–5
- Yu JG, Yu JC, Cheng B, Hark SK, Iu K (2003) The effect of F<sup>-</sup> doping and temperature on the structural and textural evolution of mesoporous TiO<sub>2</sub> powders. *J Solid State Chem* 174:372–380
- Zhang G, Li C, Cheng F, Chen J (2007) ZnFe<sub>2</sub>O<sub>4</sub> tubes: synthesis and application to gas sensors with high sensitivity and low energy consumption. *Sens Actuators B* 120:403–410

- Zhang HM, Quan X, Chen S, Zhao HM (2010) Fabrication and characterization of silica/titania nanotube composite membrane with photocatalytic capability. *Environ Sci Technol* 40:6104–6109
- Zhongshen X, Liu ZC, Xie SM, Guo J (2009) Degradation of nitrobenzene using titania photocatalyst co-doped with nitrogen and cerium under visible light illumination. *J Hazard Mater* 162:1193–1198
- Zhuang HS, Xia HL, Zhang T, Xiao DC (2008) Synthesis, characterization and visible-light photocatalytic activity of  $\text{Fe}_2\text{O}_3/\text{SnO}_2$  nanocomposites. *Mater Sci-Pol* 26:517–526
- Zou BS, Huang W, Han MY, Li SFY, Wu XC, Zhang Y, Zhang J, Zhang JS, Wu PF, Wang RY (1997) Anomalous optical properties and electron-phonon coupling enhancement in  $\text{Fe}_2\text{O}_3$  nanoparticles coated with a layer of stearates. *J Phys Chem Solids* 58:1315–1320

